Nuclear Instruments and Methods in Physics Research B 512 (2022) 42–48

Contents lists available at ScienceDirect

Nuclear Inst. and Methods in Physics Research, B

journal homepage: www.elsevier.com/locate/nimb

Atomistic simulations of acceptor removal in p-type Si irradiated with neutrons

Pedro López [a,*], María Aboy [a], Irene Muñoz [a], Iván Santos [a], Luis A. Marqués [a], Pablo Fernández-Martínez [b], Miguel Ullán [b], Lourdes Pelaz [a]

[a] ETSI Telecomunicación, Paseo de Belén 15, 47011 Valladolid, Spain
[b] Centro Nacional de Microelectrónica (IMB-CNM, CSIC), Campus UAB, 08193 Bellaterra, Barcelona, Spain

ARTICLE INFO

Keywords:
Acceptor removal
B deactivation
P-type detectors
Neutron irradiation
Displacement damage
Atomistic simulation

ABSTRACT

The effective dopant concentration in p-type Si detectors reduces with irradiation fluence at low fluences due to the acceptor removal process, which degrades detector performance and shortens its lifetime. This effect has been experimentally characterized and parametrized, but its microscopic origin is still unknown. We use atomistic simulations to gain insight into acceptor removal in neutron irradiation by modeling damage generation and defect-dopant interactions. We analyze the effect on dopant deactivation of the Si di- and tri-interstitial diffusion, the inhomogeneity of irradiation damage and the wafer temperature rise during irradiation. We characterize defect generation rates and identify the relevant defect-dopant interactions. Acceptor removal occurs mainly through the formation of B_i pairs and small boron-interstitial clusters, and it is limited by the availability of mobile Si interstitials. The presence of impurities (O, C) modifies B-complexes favoring the formation of B_iO, but has a limited effect on the amount of removed acceptors.

1. Introduction

Electronic devices operating in harsh radiative environments such as particle colliders and aerospace or nuclear applications must withstand high radiation fluences without functionality degradation. The increasing demand of radiation-hard Si detectors has motivated the recent shift from n-type to p-type substrates, as p-type sensors show a better performance under irradiation [1–3]. However, the exposure of p-type detectors to radiation results in the reduction of the effective dopant concentration (N_{eff}) with fluence at low fluences [4]. This effect is attributed to an acceptor removal process (dopant deactivation) caused by the interaction of radiation-induced defects with B atoms [5]. Acceptor removal is currently an important hurdle in the development of p-type detectors since it is responsible for the increase of substrate resistivity [4], the reduction of depletion voltage [5,6], and gain loss in active detectors [5,7].

Experimentally, N_{eff} values are mostly determined from depletion voltage measurements [6]. This is actually a measure of the space charge distribution, which reflects the concentration of active dopants that contribute as shallow acceptors, but also the presence of electrically active defects. A phenomenological description of the acceptor removal process is commonly done through a set of first order reactions between defects, dopants and impurities, using several fitting parameters that account for the amount of generated defects and the probability of defect-dopant interactions [7–9]. To simulate the electrical behavior of irradiated devices continuum models define a few energy levels in the Si bandgap that are fitted to reproduce their electrical characteristics [10,11]. Existing models offer a satisfactory fitting to some extent of the effects of irradiation on p-type detectors, but they do not provide insight into the undergoing physical mechanisms.

In this work, we use atomistic simulations to analyze the acceptor removal in neutron irradiated p-type Si by modeling damage generation and dopant deactivation process. Our damage model includes a detailed description of collision cascades, and a large number of reactions between defects and dopants are considered. We analyze the main physical mechanisms responsible for dopant deactivation and provide clues to correctly describe the acceptor removal process at atomistic level.

2. Experimental setup and simulation model

We address the study of the acceptor removal by simulating B deactivation in a radiation-hard power switch irradiated with neutrons,

* Corresponding author.
E-mail address: pedrol@ele.uva.es (P. López).

https://doi.org/10.1016/j.nimb.2021.12.003
Received 29 September 2021; Received in revised form 1 December 2021; Accepted 1 December 2021
Available online 18 December 2021

using our experimental data to validate the model. The experimental switch is designed as a set of vertical cylindrical JFET cells, which consist of a low-doped (~7.65 × 10^{13} B cm^{-3}) p-type substrate surrounded by a highly doped n-type gate [12]. To test its radiation hardness the device was irradiated with neutrons up to a 1-MeV Non-Ionizing Energy Loss (NIEL) neutron equivalent fluence (n_{eq}) of 10^{15} cm^{-2}. The irradiation campaign was carried out at the TRIGA reactor of the Jožef Stefan Institute at Ljubljana [13]. Measured drain current as a function of fluence when the switch is conducting (undepleted substrate) is reported in Fig. 1. Saturated drain current is significantly reduced for particle fluences higher than 10^{13} n_{eq} cm^{-2}, which can be explained by an increase in bulk resistivity caused by a lower N_{eff}. From these data we have estimated the N_{eff} required to obtain the resistivity values associated to the measured forward currents, also depicted in Fig. 1.

We simulate the neutron irradiation process following the schematic depicted in Fig. 2 using three different techniques. The SPECTRA-PKA code calculates the energy distribution of primary knock-on atoms (PKA) resulting from irradiation of energetic particles [14]. The MARLOWE simulator, based on the binary collision approximation, provides the coordinates of self-interstitials and vacancies generated in the collision cascades induced by PKAs [15]. Finally, the kinetic Monte Carlo tool DADOS simulates the kinetics of dopants and defects according to their thermally activated event probabilities [16,17].

Our simulation procedure comprises neutron irradiation and aging annealing processes and relies on an iterative loop that involves the tools described above. SPECTRA-PKA provides the number of PKAs generated per second and target atom in each energy slot (in this work, 10 keV energy slots are used) for 1 MeV neutron irradiation. Considering the experimental irradiation flux and the simulation cell volume, we evaluate the total number of PKAs required for each energy slot to reach a given neutron fluence. Then, a PKA energy is randomly chosen among the calculated distribution, and MARLOWE simulates the collision cascade for that PKA in pristine Si. The irradiation cascade is initiated at random within the simulation cell, and the coordinates of the new generated defects are transferred to DADOS and added to the pre-existing damage. Next, the system dynamic is simulated at the irradiation temperature for the time interval between cascades (dynamic annealing). This sequence is repeated until all PKAs for all energy slots have been simulated and the desired fluence is achieved. Once the irradiation process is over, the sample is submitted to an additional aging annealing in DADOS. This methodology allows the analysis of the effects of neutron irradiation in Si at an atomic level while, at the same time, macroscopic dimensions and timescales can be reached.

The main reactions involving defects and dopants that are relevant in neutron irradiated p-type substrates are summarized in Table 1. Point defects (PDs), i.e. Si interstitials (I's) and vacancies (V's), are mobile at

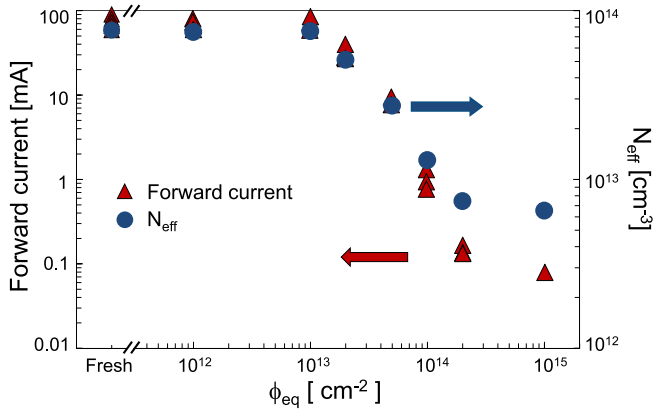

Fig. 1. Forward drain current (triangles, left axis) and estimated N_{eff} (circles, right axis) as a function of 1-MeV n_{eq} fluence, in a sample with an initial dopant concentration of 7.65 × 10^{13} B cm^{-3}.

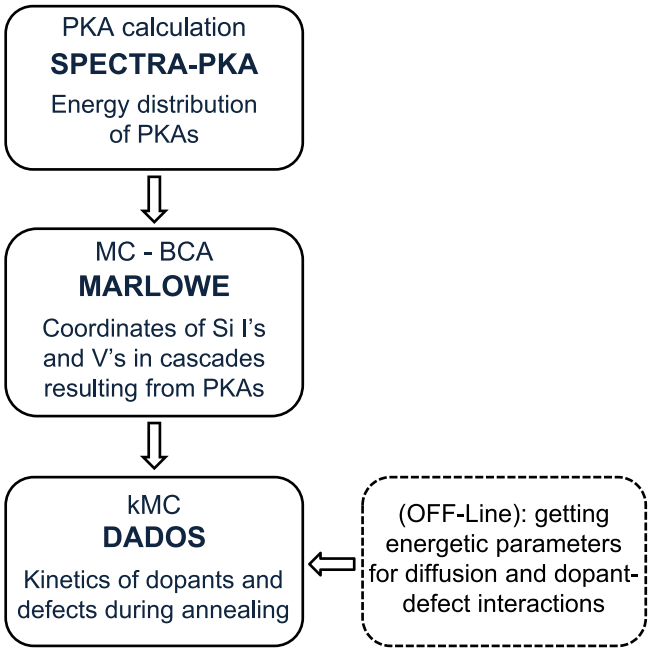

Fig. 2. Schematic of the techniques and simulation tools used in this work.

Table 1
Main equations describing defect and dopant interactions. The number of Si I's or V's belonging to a cluster is indicated by the subscript *m*, while *n* represents the number of B atoms in BICs.

(1) $I + V \rightarrow 0$	(7) $V + V_m \leftrightarrow V_{m+1}$	(13) $B_i + I_m \leftrightarrow BI_{m+1}$
(2) $I + I \leftrightarrow I_2$	(8) $I + B \leftrightarrow B_i$	(14) $I + B_nI_m \leftrightarrow B_nI_{m+1}$
(3) $I_2 + I \leftrightarrow I_3$	(9) $I_2 + B \leftrightarrow BI_2$	(15) $I_2 + B_nI_m \leftrightarrow B_nI_{m+2}$
(4) $I + I_m \leftrightarrow I_{m+1}$	(10) $I_3 + B \leftrightarrow BI_3$	(16) $I_3 + B_nI_m \leftrightarrow B_nI_{m+3}$
(5) $I_2 + I_m \leftrightarrow I_{m+2}$	(11) $B_i + B \leftrightarrow B_2I$	(17) $B_i + B_nI_m \leftrightarrow B_{n+1}I_{m+1}$
(6) $I_3 + I_m \leftrightarrow I_{m+3}$	(12) $B_i + B_i \leftrightarrow B_2I_2$	

room temperature (RT) [18] and may interact with other defects causing their mutual annihilation (equation (1) in Table 1) or the formation of clusters when defects of the same type interact. Defect clusters behave as traps for PDs as they grow in size by incorporating additional Si I's or V's (eqs. (4)-(7) in Table 1). When a Si interstitial interacts with a B atom a boron-interstitial pair (B_i) is formed (eq. (8) in Table 1). B_i can diffuse at RT [19] and interact with other B atoms or Si self-interstitials resulting in the formation of boron-interstitial clusters (BICs) (eqs. (11)–(13) in Table 1), which may contain several B atoms (n) and Si I's (m) (B_nI_m). We consider that B_i and BICs are electrically inactive as B atoms are removed from substitutional positions.

Defect energetics that govern these interactions are obtained from *ab initio* calculations or estimated by fitting experimental data. For small self-interstitial clusters we use the oscillating formation energies experimentally deduced by Cowern *et al.* [20], while for vacancy clusters we consider the values calculated by Bongiorno *et al.* from tight-binding molecular dynamics simulations [21]. BICs formation energies are taken from our atomistic model for B diffusion and clustering [22]. It is worth to note that at the temperature analyzed in this work (RT and 60 °C) defect clusters and BICs hardly dissolve, and system dynamics is mainly controlled by diffusion events and defect-dopant interactions with activation energies under ~1 eV. Most defect models assume that only single defects can diffuse, but some studies also assign a high mobility to the di-interstitial (I_2) ant tri-interstitial (I_3) defects [23,24]. In our model, we have evaluated I, I_2 and I_3 as mobile defects with migration energies of 0.9, 0.5 and 0.6 eV, respectively, in the range of literature values, similar to the migration energy of B_i pairs (0.7 eV) and slightly higher than that of V's (0.43 eV).

Simulation cells are cubic with at least $3 \times 3 \times 3$ μm^3 and periodic boundary conditions are applied in all directions. Dopant concentration is modeled by placing B atoms randomly distributed in the simulation box. We simulate 1 MeV neutron irradiation with a flux of 10^{12} cm^{-2} s^{-1} up to a maximum fluence of 10^{16} cm^{-2}. The spectrum of PKAs resulting from these irradiation conditions spans over 140 keV with an average energy of approximately 48 keV, using a uniform grid of 10 keV. The total PKA fluence in the whole energy range even for 10^{16} n cm^{-2} is only 6.15×10^{11} cm^{-2}, which is several orders of magnitude lower than the neutron fluence. In these conditions, cascade overlapping is infrequent as cascades are distant from each other even for the highest fluence (average cascade distance resulting from 10^{16} n cm^{-2} is ~ 12.8 nm). We follow the so-called CERN scenario measurement technique [25], combining irradiation steps at RT with annealing steps at 60 °C for 80 min. These aging annealings are used to accelerate system dynamics as particle detectors are designed to operate at cooled conditions for a lifetime of several years.

3. Modeling of acceptor removal

We simulate the acceptor removal process in the radiation-hard switch described before, using the same B concentration as in experiments (7.65×10^{13} cm^{-3}) and exploring irradiation fluences from 10^{12} to 10^{16} n_{eq} cm^{-2}. We will analyze the role of Si di- and tri-interstitial diffusion on simulation results, and evaluate the consequences on N_{eff} values of the wafer temperature rise during irradiation reported in experiments.

Since the availability of mobile Si I's (I_{mob}) plays a key role on B deactivation, we explore models that include the diffusion of I_2 and I_3 defects. Being I_2 and I_3 highly mobile at RT, their interactions with other defects and dopants (reported in Table 1) have an impact on system evolution and in particular on N_{eff}. We show in Fig. 3 the relative effective dopant concentration ($N_{eff}/N_{eff,0}$), i.e. the ratio of the effective dopant concentration to the value before irradiation ($N_{eff,0}$), as a function of neutron fluence. In our simulations, N_{eff} represents the concentration of substitutional B atoms, which are assumed to be electrically active. Simulation results correspond to damage models including the diffusion of only the single Si self-interstitial (I) (I_2 and I_3 being immobile), the diffusion of both single and di-interstitial (I-I_2) and the diffusion of all single, di- and tri-interstitial (I-I_2-I_3). The experimental $N_{eff}/N_{eff,0}$ is also depicted in the figure, calculated from N_{eff} values reported in Fig. 1. Compared to the I-diffusion model, the inclusion of I_2 and I_3 as mobile defects results in higher B deactivation and $N_{eff}/N_{eff,0}$ values closer to the experimental ones, as the diffusion of I_2 and I_3 opens new pathways for B deactivation (eqs. (9)-(10) in Table 1). For the highest fluence, 19% of B atoms still remain active for the I-I_2-I_3 diffusion model, a value slightly higher than the experimental one (9%). These results evidence that the mobility of small interstitials defects (I_2 and I_3) plays a significant role in B deactivation in irradiated devices around RT. Therefore, all the subsequent simulations will consider the diffusion of all three mobile species.

Simulation results for the I-I_2-I_3 diffusion model shown in Fig. 3 were fitted to an exponential decay equation in the so called "Hamburg model" [26],

$$N_{eff}(\phi_{eq}) = N_{eff,0} - N_C\left[1 - exp\left(-c_A\phi_{eq}\right)\right] \quad (1)$$

in which ϕ_{eq} is the 1-MeV neutron NIEL equivalent fluence, $N_{eff,0}$ the initial acceptor concentration, N_C the concentration of removed acceptors and c_A the acceptor removal constant. The extracted c_A value 1.18×10^{-14} cm^2 is in the range of those reported in literature for a similar $N_{eff,0}$ [7].

Particle detectors must withstand radiation for a lifetime of several years, which may lead to large accumulated fluences. Detector radiation hardness is commonly tested in accelerated experiments that combine neutron irradiation and aging annealings, but irradiation fluxes are much higher than those for detector operational conditions [27]. Irradiation in neutron reactors unavoidably results in wafer heating especially for high fluxes and fluences, which can be mitigated to some extent with proper cooling systems. Experiments of neutron irradiation at RT at the JSI TRIGA reactor report a sample temperature that may reach 45–65 °C, depending on reactor power and the channel at which the sample is located [27,28]. This temperature fluctuation adds uncertainty to experimental results and may play a role in acceptor removal, as system dynamics is controlled by thermally activated processes. In a recent study, a wide range of neutron irradiation fluxes was used, which resulted in different wafer temperatures, but detector performance was not significantly altered [27].

To quantify the effect of the wafer temperature rise on dopant deactivation, we have simulated neutron irradiation at different temperatures. After each irradiation step, the sample is annealed at 60 °C for 80 min as described before. We have depicted in Fig. 4 the relative effective dopant concentration as a function of fluence in samples irradiated at 25 °C, 50 °C and 75 °C, covering the temperature fluctuation of experiments. Temperature increase results in a slightly lower N_{eff} just after irradiation steps, but similar N_{eff} values are observed after irradiation and annealing. The temperature rise enhances Si I's diffusion and therefore dopant deactivation, resulting in a lower N_{eff} when irradiation is over. However, wafer temperatures reported in irradiation experiments are similar to the aging annealing temperature and, consequently,

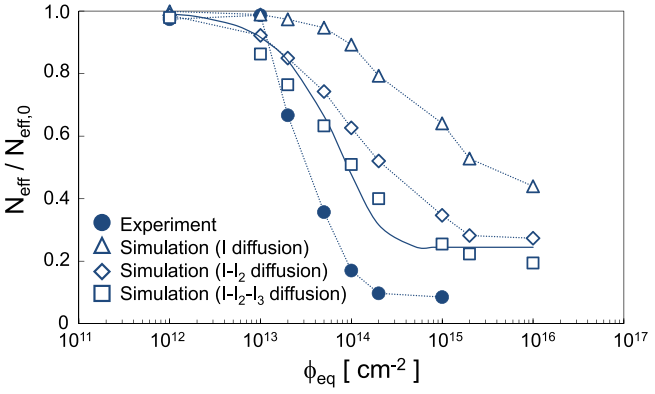

Fig. 3. Dependence of $N_{eff}/N_{eff,0}$ on the accumulated 1-MeV n_{eq} fluence. Experimental N_{eff} was extracted from Fig. 1. Simulated values correspond to active B resulting from damage models including the diffusion of the single self-interstitial (I), the I and I_2 defects (I-I_2), and all the I, I_2 and I_3 defects (I-I_2-I_3). A solid line shows the fitting of the I-I_2-I_3 model data to equation (1). Dotted lines are guides to the eye.

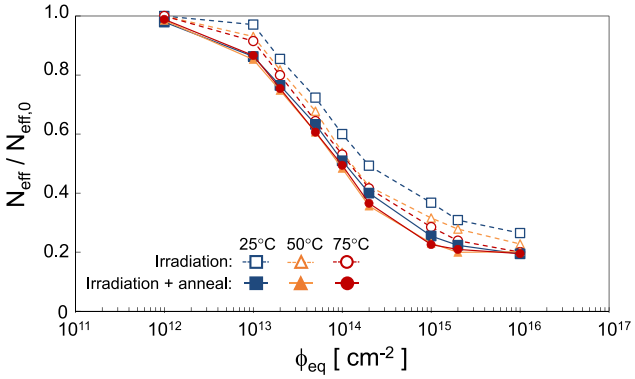

Fig. 4. Simulated $N_{eff}/N_{eff,0}$ as a function of 1-MeV n_{eq} fluence, after irradiation steps (open symbols) and after irradiation and anneal steps (solid symbols). Irradiation was done at 25 °C (blue), 50 °C (orange) and 75 °C (red). (For interpretation of the references to colour in this figure legend, the reader is referred to the web version of this article.)

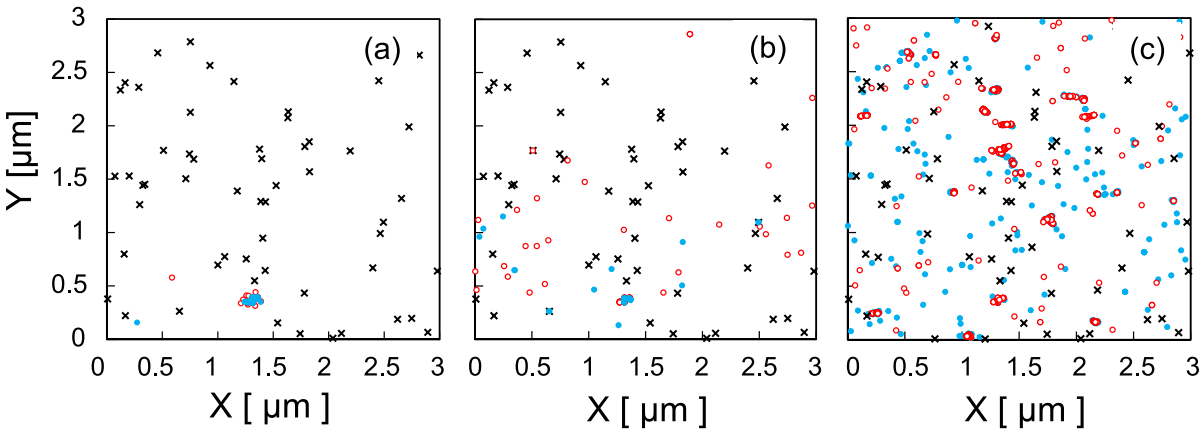

Fig. 5. Distribution of Si I's (solid circles), V's (open circles) and B atoms (crosses) after irradiation steps in samples with 7.65 × 10^{13} B cm^{-3} irradiated with 10^{12} (a), 10^{13} (b) and 10^{14} (c) 1-MeV n_{eq} cm^{-2}. The plots are projections over 100 nm of depth (Z).

the effect of the temperature rise during irradiation is overcome by the intensity of the subsequent annealing.

4. Neutron irradiation damage

The atomistic description of damage in our simulations allows us to explore the defect distribution resulting from neutron irradiation, which is key to understand the dependence of N_{eff} on fluence. In Fig. 5 we plot the positions of Si I's, V's and B atoms in a sample with 7.65 × 10^{13} B cm^{-3} after irradiation with 10^{12}, 10^{13} and 10^{14} 1-MeV n_{eq} cm^{-2}. B atoms are randomly distributed while Si I's and V's are mainly concentrated in regions along the recoil track. 1 MeV neutron interaction with Si is characterized by head-on collisions resulting in 50 keV PKAs on average that produce dense damaged regions [29,30]. As PKA fluence is several orders of magnitude lower than the neutron irradiation fluence, collision cascades may be quite distant to each other, especially at low fluences. Note that defects and dopants may be more distant than they appear in the figure as plots are 2D projections over 100 nm of depth. Defects are more abundant and cascades are closer to each other as fluence increases. Because of the inhomogeneity of damage distribution, Si I's are more likely to interact with intra-cascade defects (being recombined with V's or trapped in Si I's clusters), and only a small fraction escape and interact with B atoms.

We have quantified the damage resulting from 1 MeV neutron irradiation, for the sample doped with 7.65 × 10^{13} B cm^{-3} and for a blank sample with no dopants, as shown in Fig. 6. In these simulations, the sample was irradiated up to an accumulated fluence of 10^{16} n_{eq} cm^{-2}, but no aging annealing was done. The generation rate of displacement damage, defined as the ratio of defect concentration to irradiation fluence, has a constant value of 184 cm^{-1}. This accounts for the amount of Si I's and V's resulting directly from irradiation cascades and depends only on the number and energy of PKAs. We have included in the figure the generation rate of mobile Si I's ($g_{I,mob}$) and that of clusters of Si I's and V's ($g_{I,V,clusters}$) calculated for the blank and B-doped samples after irradiation. The amount of remaining defects after irradiation is notably smaller than that of generated defects. This evidences that intense I-V recombination within the collision cascade has occurred during the dynamic annealing of RT irradiation. The survival rate of Si I's to recombination, calculated as the fraction of Si I's still remaining (as PDs or in clusters) after each irradiation step, is also depicted. The survival rate decreases with fluence because the existence of more damage and the closeness of cascades favor defect recombination. Both $g_{I,mob}$ and $g_{I,V,clusters}$ also reduce with fluence, which means that defect concentration undergoes a sublinear growth with fluence, caused by the enhanced I-V recombination at large fluences. $g_{I,V,clusters}$ decreases at a slower pace than $g_{I,mob}$ as the progressive damage accumulation with fluence increases the probability of Si I's being trapped in clusters.

The generation rate of interstitial PDs in irradiated p-type Si has been experimentally reported in the range of 1–3 cm^{-1} [31,32]. However, according to a recent analysis of acceptor removal based on defect kinetic equations, generation rates over one order of magnitude higher were needed to explain the removal process [9]. Besides, there is an open question on whether these rates depend on substrate resistivity. Our results show that $g_{I,mob}$ strongly depends on irradiation fluence. For the highest fluence, a value in the range of the experimental ones is obtained (~1.8 cm^{-1}), but for the lowest fluence $g_{I,mob}$ is almost 10 times higher (~17 cm^{-1}). Data reported in Fig. 6 for the blank sample and that doped with 7.65 × 10^{13} B cm^{-3} show the same trend, which suggests that $g_{I,mob}$ does not depend on substrate resistivity.

Only those mobile Si I's that have survived recombination and trapping could potentially scape from irradiation cascades and eventually reach and interact with B atoms. The concentration of I_{mob} after irradiation and that of removed acceptors (N_C) after irradiation and annealing is plotted in Fig. 7 as a function of fluence. The ratio $N_C/N_{eff,0}$ is also shown (right axis). At low fluences, the concentration of I_{mob} is comparable of even smaller than $N_{eff,0}$ (dashed line) and the amount of removed acceptors is small. For higher fluences, the concentration of I_{mob} clearly exceeds $N_{eff,0}$ resulting in a fast increase in N_C. For fluences above 10^{15} n_{eq} cm^{-2} N_C saturates at approximately 80% of $N_{eff,0}$. The relative amount of I_{mob} compared to $N_{eff,0}$ provides the clues to understand N_{eff} dependence with fluence. When the irradiation fluence is low,

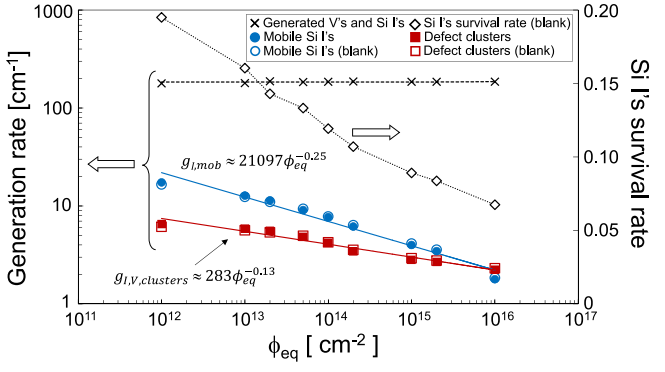

Fig. 6. Generation rate of I_{mob} ($g_{I,mob}$), and Si I's and V's clusters ($g_{I,V,clusters}$) after irradiation as a function of fluence. Solid symbols correspond to the sample with 7.65 × 10^{13} B cm^{-3} and empty symbols to a blank sample. Solid lines are the best fit of the B-doped sample data to a power equation. The generation rate of displacement damage (Si I's and V's) is plotted as crosses, and the survival rate of Si I's after irradiation in the blank sample as open diamonds (right axis).

the small number of mobile Si I's limits the removal process. For higher fluences, mobile Si I's are abundant and B deactivation is greatly enhanced resulting in a fast decay of N_{eff} with fluence. The incomplete removal observed at the highest fluences indicates a reduced efficiency on the removal process, as some B atoms remain substitutional despite the large population of I_{mob}. As shown in Fig. 6, at high fluences the concentration of Si I's and V's clusters exceeds that of mobile Si I's and is much higher than $N_{eff,0}$, which makes that I_{mob} are more likely to interact with clusters instead of reaching B atoms.

5. B deactivation mechanisms and the role of O and C

Acceptor removal may occur through different pathways that lead to the formation of B_i and BICs, which may include B_1I_2, B_1I_3 and potentially higher order BICs through reactions of preexisting BICs with mobile Si I's or B_i. Thermal stability of deactivated B is determined by the predominance of B_i or BICs, and by the stoichiometry of BICs, i.e. the number of B atoms and Si I's they contain. The availability and distribution of I_{mob} together with the dopant concentration will define the dominant reactions. In Fig. 8 we report the fraction of deactivated B (N_C) that corresponds to B_i and BICs, and the relative weight on N_C of BICs with 1 (B_1I_m) or 2 (B_2I_m) B atoms, for the sample with 7.65×10^{13} B cm^{-3} after 10^{16} n_{eq} cm^{-2} irradiation. The average ratio of Si I's/B atoms contained in BICs is also depicted (right axis). At low fluences, deactivated B corresponds mainly to B_1I_m while B_i represents only 24% of N_C. At high fluences, N_C is equally distributed between B_i and BICs that are mostly B_1I_m.

B deactivation is initiated with the interaction of a mobile Si interstitial (I, I_2, I_3) with a substitutional B atom and the formation of B_i, B_1I_2 and B_1I_3, respectively. At low fluences, when there is a limited number of I_{mob}, the fastest diffusers (I_2 and I_3) are more likely to leave irradiation cascades and interact with B resulting in B_1I_m clusters. As the number of I_{mob} increases with fluence, the diffusion of the single Si interstitial and the formation of B_i significantly contributes to acceptor removal. The predominance of B_1I_m and the average ratio of ~2.4 Si I's per B atom in BICs indicate that BICs mostly correspond to B_1I_2 and B_1I_3. The relative population of B_i and BICs, and BIC stoichiometry, may differ for other $N_{eff,0}$ values. It must be remarked that, contrary to the phenomenological description of acceptor removal, our model considers all reactions leading to the formation and growth of B_i and BICs with any stoichiometry, providing a full atomistic description of defect-dopant interactions.

Si wafers are usually contaminated with impurities such as oxygen and carbon. Impurity concentration strongly depends on the growth technique but, for standard Si, concentrations of 10^{15}–10^{17} O cm^{-3} and 10^{15}–10^{16} C cm^{-3} are commonly found [30,33]. These values are comparable or even higher than typical $N_{eff,0}$ in p-type detectors. O and C can interact with intrinsic defects and dopants: O reacts mainly with

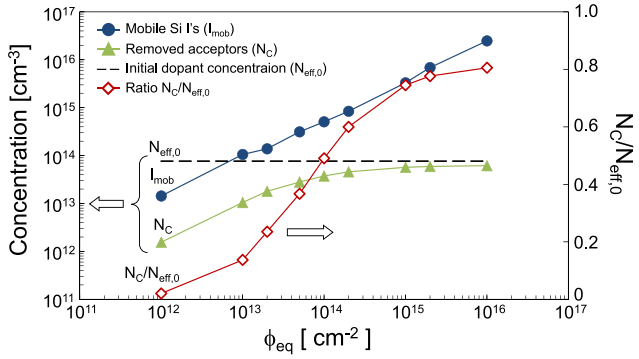

Fig. 7. Concentration of I_{mob} (circles) after irradiation and N_C after irradiation and anneal (triangles) as a function of fluence. The dashed line shows the value of $N_{eff,0}$. The ratio $N_C/N_{eff,0}$ is plotted as diamonds (right axis).

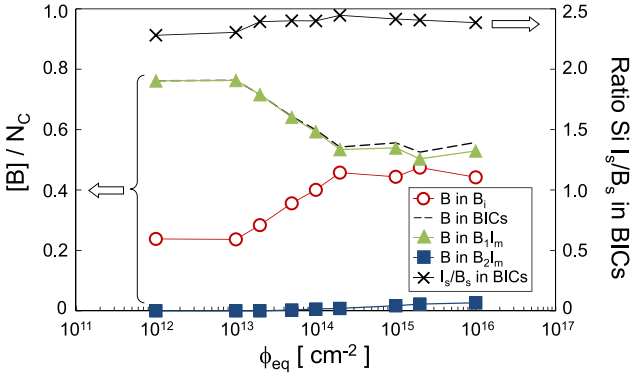

Fig. 8. Fraction of deactivated B via the formation of B_i (open circles) and BICs (dashed line) as a function of fluence. Solid symbols represent the fraction of deactivated B belonging to B_1I_m (triangles) and B_2I_m (squares). Black crosses show the average ratio of the number of Si I's to that of B atoms contained in BICs.

Table 2
Equations describing the main interactions between intrinsic defects and impurities (O, C) and the formation of the B_iO complex.

(1) $V + O \leftrightarrow VO$	(3) $VO + I_2 \leftrightarrow O + I$	(5) $C + I \leftrightarrow C_i$	(7) $B_i + O \leftrightarrow B_iO$
(2) $VO + I \leftrightarrow O$	(4) $VO + I_3 \leftrightarrow O + I_2$	(6) $C_i + V \leftrightarrow C$	(8) $B_iO + V \leftrightarrow B + O$

V's resulting in VO pairs and other V-O complexes [34], while C captures Si I's forming C_i pairs and C-I complexes [35]. Several reports in literature suggest a strong affinity of B_i for O, and point out the B_iO complex as a main actor in acceptor removal [36,37]. The presence of O and C concentrations comparable to $N_{eff,0}$, and their interactions with defects and dopants may have an impact on dopant deactivation.

We have included the role of O and C in our model by considering the formation of VO, C_i and B_iO defects. All of them are assumed to be immobile, and they behave as traps by capturing V's, Si I's and B_i, respectively. Table 2 summarizes the main equations that lead to the formation and dissolution of VO, C_i and B_iO defects. A new simulation was done for a sample with 7.65×10^{13} B cm^{-3} enriched with 10^{17} O cm^{-3} and 2×10^{15} C cm^{-3}. O concentration is much higher than $N_{eff,0}$ and exceeds that of C to appreciate its effect. The fraction of active B and deactivated B via the formation of B_i, BICs and B_iO complexes is plotted in Fig. 9. The presence of O and C hardly modifies the overall amount of active B, and only at large irradiation fluences a slightly higher B deactivation is observed. However, the distribution of deactivated B is

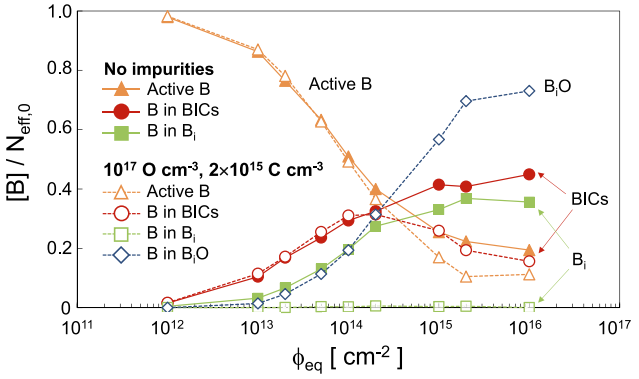

Fig. 9. Fraction of B atoms in substitutional positions (active B) (triangles), belonging to BICs (circles), B_i (squares) and B_iO complexes (diamonds) as a function of fluence. Data correspond to simulations without impurities (solid symbols and lines), and with 10^{17} O cm^{-3} and 2×10^{15} C cm^{-3} (open symbols and dashed lines).

significantly altered. B_i has almost disappeared because once mobile B_i are formed, they easily interact with the high concentration of O resulting in B_iO complexes. Besides, at high fluences, the enhanced recombination of I_2 and I_3 defects at VO pairs hinders the formation of BICs in favor of B_iO complexes.

6. Conclusions

Atomistic simulations are used to analyze the acceptor removal process in neutron irradiated p-type Si by modeling damage generation and defect-dopant interactions. Our simulations correctly describe the reduction of N_{eff} with fluence associated to the interaction of B atoms with mobile Si I's, which includes the diffusion of I, I_2 and I_3 defects. Acceptor removal is controlled by the availability of mobile Si I's and the probability of I-B interaction. These factors are limited by the intense I-V recombination and trapping at defect clusters within irradiation cascades derived from the inhomogeneity of neutron irradiation damage. The presence of impurities, and in particular a high O concentration, modifies the composition of B related defects responsible for B deactivation, favoring the formation of B_iO complexes, but has little effect on the overall amount of active B.

Declaration of Competing Interest

The authors declare that they have no known competing financial interests or personal relationships that could have appeared to influence the work reported in this paper.

Acknowledgements

This work has been supported by the Spanish Ministerio de Ciencia e Innovación under Project No. PID2020-115118GB-I00.

References

[1] W. Adam, et al., P-type silicon strip sensors for the new CMS Tracker at HL-LHC, J. Instrum. 12 (2017) 06018, https://doi.org/10.1088/1748-0221/12/06/P06018.
[2] M. Moll, Recent advances in the development of radiation tolerant silicon detectors for the super-LHC, in: Astroparticle, Particle and Space Physics, Detectors and Medical Physics Applications, World Scientific, Singapore, 2011, pp. 101–110, https://doi.org/10.1142/9789814307529_0018.
[3] A. Affolder, P. Allport, G. Casse, Charge collection efficiencies of planar silicon detectors after reactor neutron and proton doses up to 1.6×10^{16} n_{eq} cm^{-2}, Nucl. Instrum. Methods Phys. Res., Sect. A 612 (3) (2010) 470–473, https://doi.org/10.1016/j.nima.2009.08.005.
[4] R. Wunstorf, W.M. Bugg, J. Walter, F.W. Garber, D. Larson, Investigations of donor and acceptor removal and long term annealing in Si with different boron/phosphorous ratios, Nucl. Instrum. Meth. Phys. Res. A 377 (1996) 228–233, https://doi.org/10.1016/0168-9002(96)00217-3.
[5] G. Kramberger, M. Carulla, E. Cavallaro, V. Cindro, D. Flores, Z. Galloway, S. Grinstein, S. Hidalgo, V. Fadeyev, J. Lange, I. Mandić, G. Medin, A. Merlos, F. McKinney-Martinez, M. Mikuž, D. Quirion, G. Pellegrini, M. Petek, H.F.-W. Sadrozinski, A. Seiden, M. Zavrtanik, Radiation hardness of thin Low Gain Avalanche Detectors, Nuclear Inst. Methods Phys. Res., A 891 (2018) 68–77, https://doi.org/10.1016/j.nima.2018.02.018.
[6] V. Cindro, G. Kramberger, M. Lozano, I. Mandić, M. Mikuž, G. Pellegrini, J. Pulko, M. Ullan, M. Zavrtanik, Radiation damage in p-type silicon irradiated with neutrons and protons, Nucl. Instrum. Meth. Phys. Res. A 599 (1) (2009) 60–65, https://doi.org/10.1016/j.nima.2008.11.007.
[7] M. Ferrero, R. Arcidiacono, M. Barozzi, M. Boscardin, N. Cartiglia, G.F.D. Betta, Z. Galloway, M. Mandurrino, S. Mazza, G. Paternoster, F. Ficorella, L. Pancheri, H.-F.W. Sadrozinski, F. Siviero, V. Sola, A. Staiano, A. Seiden, M. Tornago, Y. Zhao, Radiation resistant LGAD design, Nucl. Instrum. Meth. Phys. Res. A 919 (2019) 16–26, https://doi.org/10.1016/j.nima.2018.11.121.
[8] M. Centis, Acceptor Removal Parametrization-thoughts-, 35th RD50 Workshop on Radiation hard semiconductor devices for very high luminosity colliders, Zurich, Switzerland, Nov. 2019. [Online]. Available: https://indico.cern.ch/event/855994/.
[9] M. Moll, Acceptor removal - Displacement damage effects involving the shallow acceptor doping of p-type silicon devices, Proc. of Science 373, 027 – The 28th International Workshop on Vertex Detectors (Vertex2019) – Radiation effects, https://doi.org/10.22323/1.373.0027. [Online] Available: https://pos.sissa.it/373/027/.
[10] F. Moscatelli, D. Passeri, A. Morozzi, R. Mendicino, G.-F. Dalla Betta, G.M. Bilei, Combined bulk and surface radiation damage effects at very high fluences in silicon detectors: measurements and TCAD simulations, IEEE Trans. Nucl. Sci. 63 (5) (2016) 2716–2723, https://doi.org/10.1109/TNS.2016.2599560.
[11] R. Dalal, A. Bhardwaj, K. Ranjan, K. Lalwani, G. Jain, Simulation of irradiated Si detectors, Proceedings of Science 227, 030 – The 23rd International Workshop on Vertex Detectors (Vertex2014) - R&D and Detector Simulations, https://doi.org/10.22323/1.227.0030. [Online] Available: https://pos.sissa.it/227/030/.
[12] P. Fernández-Martínez, D. Flores, S. Hidalgo, X. Jordà, X. Perpiñà, D. Quirion, L. Ré, M. Ullán, M. Vellvehí, A new vertical JFET power device for harsh radiation environments, Energies 10 (2017) 256, https://doi.org/10.3390/en10020256.
[13] L. Snoj, G. Žerovnik, A. Trkov, Computational analysis of irradiation facilities at the JSI TRIGA reactor, Appl. Radiat. Isot. 70 (2012) 483, https://doi.org/10.1016/j.apradiso.2011.11.042.
[14] M.R. Gilbert, J. Marian, J.-Ch. Sublet, Energy spectra of primary knock-on atoms under neutron irradiation, J. Nucl. Mat. 467 (2015) 121–134, https://doi.org/10.1016/j.jnucmat.2015.09.023.
[15] M.T. Robinson, I.M. Torrens, Computer simulation of atomic displacement cascades in solids in the binary-collision approximation, Phys. Rev. B 9 (12) (1974) 5008–5024, https://doi.org/10.1103/PhysRevB.9.5008.
[16] M. Aboy, L. Pelaz, L.A. Marqués, P. López, J. Barbolla, R. Duffy, Atomistic analysis of the evolution of boron activation during annealing in crystalline and preamorphized silicon, J. Appl. Phys. 97 (103520) (2005) 1–7, https://doi.org/10.1063/1.1904159.
[17] L. Pelaz, M. Jaraiz, G.H. Gilmer, H.-J. Gossmann, C.S. Rafferty, D.J. Eaglesham, J. M. Poate, B diffusion and clustering in ion implanted Si: the role of B cluster precursors, Appl. Phys. Lett. 70 (17) (1997) 2285–2287, https://doi.org/10.1063/1.118839.
[18] K.K. Larsen, V. Privitera, S. Coffa, F. Priolo, S.U. Campisano, A. Carnera, Trap-limited migration of Si self-interstitials at room temperature, Phys. Rev. Lett. 76 (1996) 1493, https://doi.org/10.1103/PhysRevLett.76.1493.
[19] E. Napolitani, D. de Salvador, R. Storti, A. Carnera, S. Mirabella, F. Priolo, Room temperature migration of boron in crystalline silicon, Phys. Rev. Lett. 93 (2004), 055901, https://doi.org/10.1103/PhysRevLett.93.055901.
[20] N.E.B. Cowern, G. Mannino, P.A. Stolk, F. Roozeboom, H.G.A. Huizing, J.G.M. van Berkum, F. Cristiano, A. Claverie, M. Jaraíz, Energetics of self-interstitial clusters in Si, Phys. Rev. Lett. 82 (22) (1999) 4460–4463, https://doi.org/10.1103/PhysRevLett.82.4460.
[21] A. Bongiorno, L. Colombo, T.D.de la Rubia, Structural and binding properties of vacancy clusters in silicon, Europhys. Lett. 43 (6) (1998) 695–700, https://doi.org/10.1209/epl/i1998-00419-1.
[22] M. Aboy, L. Pelaz, E. Bruno, S. Mirabella, S. Boninelli, Kinetics of large B clusters in crystalline and preamorphized silicon, J. Appl. Phys. 110 (2011), 073524, https://doi.org/10.1063/1.3639280.
[23] S.K. Estreicher, M. Gharaibeh, P.A. Fedders, P. Ordejon, Unexpected dynamics for self-interstitial clusters in silicon, Phys. Rev. Lett. 86 (2001) 1247, https://doi.org/10.1103/PhysRevLett.86.1247.
[24] M. Posselt, F. Gao, D. Zwicker, Atomistic study of the migration of di- and tri-interstitials in silicon, Phys. Rev. B 71 (2005), 245202, https://doi.org/10.1103/PhysRevB.71.245202.
[25] A. Ruzin, Recent results from the RD-48 (ROSE) collaboration, Nucl. Instrum. Meth. Phys. Res. A 447 (1-2) (2000) 116–125, https://doi.org/10.1016/S0168-9002(00)00179-0.
[26] M. Moll, E. Fretwurst, G. Lindström, Investigation on the improved radiation hardness of silicon detectors with high oxygen concentration, Nucl. Instrum. Meth. Phys. Res. A 439 (2-3) (2000) 282–292, https://doi.org/10.1016/S0168-9002(99)00842-6.
[27] A. Howard, V. Cindro, B. Hiti, G. Kramberger, Ž. Kljun, G. Laštovička-Medin, I. Mandić, M. Mikuž, Dependence of Low Gain Avalanche Detectors performance on neutron flux, Nucl. Instrum. Meth. Phys. Res. A 996 (2021), 165160, https://doi.org/10.1016/j.nima.2021.165160.
[28] V. Cindro, et al., Measurement of the charge collection in irradiated miniature sensors for the upgrade of the ATLAS phase-II strip tracker, Nucl. Instrum. Meth. Phys. Res. A 924 (2019) 153–159, https://doi.org/10.1016/j.nima.2018.10.007.
[29] M. Huhtinen, Simulation of non-ionising energy loss and defect formation in silicon, Nucl. Instrum. Meth. Phys. Res. A 491 (1-2) (2002) 194–215, https://doi.org/10.1016/S0168-9002(02)01227-5.
[30] I. Pintilie, G. Lindstroem, A. Junkes, E. Fretwurst, Radiation induced point and cluster-related defects with strong impact to damage properties of silicon detectors, Nucl. Instrum. Meth. Phys. Res. A 611 (2009) 52–68, https://doi.org/10.1016/j.nima.2009.09.065.
[31] G. Davies, S. Hayama, L. Murin, R. Krause-Rehberg, V. Bondarenko, A. Sengupta, C. Davia, A. Karpenko, Radiation damage in silicon exposed to high-energy protons, Phys. Rev. B 73 (2006), 165202, https://doi.org/10.1103/PhysRevB.73.165202.
[32] M. Moll, PhD thesis, Radiation Damage in Silicon Particle Detectors – microscopic defects and macroscopic properties -, Hamburg University, 1999.
[33] G. Lindström, et al., Radiation hard silicon detectors—developments by the RD48 (ROSE) collaboration, Nucl. Instrum. Meth. Phys. Res. A 466 (2) (2001) 308–326, https://doi.org/10.1016/S0168-9002(01)00560-5.
[34] J.L. Lindström, L.I. Murin, V.P. Markevich, T. Hallberg, B.G. Svensson, Vibrational absorption from vacancy-oxygen-related complexes (VO, V_2O, VO_2) in irradiated silicon, Physica B 273–274 (1999) 291–295, https://doi.org/10.1016/S0921-4526(99)00447-0.

[35] P.A. Stolk, D.J. Eaglesham, H.-J. Gossmann, J.M. Poate, Carbon incorporation in silicon for suppressing interstitial-enhanced boron diffusion, Appl. Phys. Lett. 66 (1995) 1370, https://doi.org/10.1063/1.113204.
[36] L.C. Kimerling, M.T. Asom, J.L. Benton, P.J. Drevinsky, C.E. Caefer, Interstitial defect reactions in silicon, Mater. Sci. Forum 38–41 (1989) 141–150, https://doi.org/10.4028/www.scientific.net/msf.38-41.141.
[37] P.M. Mooney, L.J. Cheng, M. Süli, J.D. Gerson, J.W. Corbett, Defect energy levels in boron-doped silicon irradiated with 1-MeV electrons, Phys. Rev. B 15 (1977) 3836, https://doi.org/10.1103/PhysRevB.15.3836.